HHS Public Access

Author manuscript

J Immunol. Author manuscript; available in PMC 2020 August 15.

Published in final edited form as:

J Immunol. 2019 August 15; 203(4): 936–945. doi:10.4049/jimmunol.1900093.

THE IMPACT OF TCR SIGNAL STRENGTH ON RESIDENT MEMORY T CELL FORMATION DURING INFLUENZA VIRUS INFECTION

Jessica K. Fiege[*], **Ian A. Stone**[*], **Elizabeth J. Fay**[*,†], **Matthew W. Markman**[*], **Sathi Wijeyesinghe**[*], **Marissa G. Macchietto**[‡], **Steven Shen**[‡], **David Masopust**[*], **Ryan A. Langlois**[*,†,¶]

[*]Department of Microbiology and Immunology and the Center for Immunology, University of Minnesota, Minneapolis, MN, 55455

[†]Biochemistry, Molecular Biology and Biophysics Graduate Program, University of Minnesota, Minneapolis, MN, 55455

[‡]Institute for Health Informatics, University of Minnesota, Minneapolis, MN, 55455

Abstract

Resident memory T (T_{RM}) cells in the lung are vital for heterologous protection against influenza A virus (IAV). Environmental factors are necessary to establish lung T_{RM}, however the role of T cell intrinsic factors like T cell receptor (TCR) signal strength have not been elucidated. Here we investigated the impact of TCR signal strength on the generation and maintenance of lung T_{RM} cells after IAV infection. We inserted high and low affinity OT-I epitopes into IAV and infected mice after transfer of OT-I T cells. We uncovered a bias in T_{RM} formation in the lung elicited by lower affinity TCR stimulation. TCR affinity did not impact the overall phenotype or long-term maintenance of lung T_{RM} cells. Overall, these findings demonstrate that T_{RM} formation is negatively correlated with increased TCR signal strength. Lower affinity cells may have an advantage in forming T_{RM} to ensure diversity in the antigen-specific repertoire in tissues.

INTRODUCTION

Following infection, naïve antigen specific-$CD8^+$ T cells are primed in secondary lymphoid organs (SLOs) by antigen-bearing dendritic cells (DCs). These antigen-specific $CD8^+$ T cells rapidly expand, differentiate, and traffic to the site of infection. After contraction a proportion survive to become memory cells which can be subdivided into three broad subsets. Two subsets are present primarily in the circulation, and can be distinguished by the expression of CD62L. Effector memory T (T_{EM}) cells lack CD62L expression and

[¶]Corresponding Author: Ryan A. Langlois, Phone: 612-625-3633, Fax: 612-626-0623, langlois@umn.edu.

Author Contributions

RAL and JKF designed and conceived of the study. JKF, IAS, EJF, SW performed experiments and analyzed data. MWM, MGM and SS analyzed RNA-seq data. DM helped design experiments and interpret results. JKF and RAL wrote the manuscript. All authors contributed to the final editing of the manuscript. RAL supervised the study.

Disclosure

The authors declare no conflicts of interests

preferentially circulate through the blood, splenic red pulp and non-lymphoid tissues (NLTs) (1). Central memory T (T_{CM}) cells express CD62L and circulate through SLOs and the blood (1). The third memory population, tissue resident memory T (T_{RM}) cells, reside in NLTs and are poised to rapidly respond to a secondary infection (2). T_{RM}s can mediate protection against many virus infections and are critical for control of reinfection with influenza A viruses (IAVs) (3–6). While T_{RM} cells in most NLTs appear durable (7–9), T_{RM} cells in the lung wane rapidly with negative consequences for protection against IAV (3–6). Understanding the intrinsic and extrinsic signals that drive formation and maintenance of lung T_{RM} cells will be critical for the design of broadly protective durable IAV vaccines.

Environmental cues are critical drivers of establishing T_{RM} cells (5, 10–12). While some environmental cues needed for T_{RM} formation are known, there may also be a role for cell intrinsic signals. T_{RM} cells are also impacted by antigen presentation and T_{RM} formation in the lung may require local antigen (13–16). In addition to antigen presentation, TCR affinity has been demonstrated to shape memory $CD8^+$ T cell differentiation. Higher affinity TCR interactions push $CD8^+$ T cells towards a T_{EM} cell fate, while reduced TCR affinity stimulation preferentially generates T_{CM} cells (17). Given that T_{RM} share some traits with T_{EM} cells (10), it is possible that high affinity simulation will favor T_{RM}. Conversely, TCR signal strength was shown to be inversely correlated with T_{RM} in the brain (18). However, a separate study found that brain T_{RM} cells had overall higher affinity TCR than peripheral memory counterparts (19). Together these data highlight the potential impacts of TCR affinity in the differentiation of T_{RM}. However, the consensus rules of how TCR affinity effects T_{RM} ontogeny are not yet clear, and this issue has not been investigated in the lung or other mucosal tissues.

To investigate the role of TCR signal strength in T_{RM} cell formation after IAV infection we generated viruses expressing the cognate antigen for OT-I T cells, $OVA_{257–264}$ SIINFEKL (N4) peptide, or altered peptide ligands (APLs) with reduced affinity. B6 mice bearing naïve OT-I T cells were infected with IAVs containing OT-I epitopes and lung T_{RM} cell formation was assessed. Consistent with published reports, affinity correlated with clonal burst size (20). As expected, cells stimulated by higher affinity ligands also were more likely to form T_{EM} than T_{CM}. Interestingly, decreased affinity stimulated $CD8^+$ T cells had an advantage in forming T_{RM} in the lung. Transcriptional profiling demonstrates that low affinity stimulated cells have increased survival factors suggesting a potential mechanism for the disparity. Though low affinity cells were more likely to form T_{RM}, high and low affinity T_{RM} cells exhibited similar phenotypes and functions. These data suggest that in addition to environmental cues, TCR affinity also has a significant impact on programing T_{RM} differentiation. This is consistent with a model where terminal differentiation negatively impacts T_{RM}, shedding new light on the ontogeny of T_{RM}.

MATERIALS AND METHODS

Mice

Female C57Bl/6 mice were purchased from The Jackson Laboratory. CD45.1 OT-I TCR-Tg mice were provided by Dr. Vezys (University of Minnesota). All experimental protocols

involving the use of mice were approved by the Institutional Animal Care and Use Committee at the University of Minnesota.

Flow cytometry and reagents

Single cell suspensions were washed with 1 X PBS and stained with a fixable viability dye for 30 min on ice, Ghost Dye™ Red 780 or UV 450 (Tonbo). Cells were washed once with FACS buffer (cold HBSS supplemented with 2% bovine serum), stained with surface Abs, then washed before flow cytometric detection on a BD LSRFortessa (Becton Dickinson). For IFN-γ staining, spleen and lung single cell suspensions were incubated in complete T cell media with/without 1 or 0.1 μg/mL SIINFEKL or SIITFEKL peptides for 4 h at 37° in the presence of GolgiPlug (BD Biosciences). For positive intracellular staining controls, cells were stimulated with eBioscience™ Cell Stimulation Cocktail. Cells were washed 2x with FACS buffer and stained as above. For intracellular staining cells were fixed with BD Cytofix/Cytoperm (BD Biosciences), incubated on ice for 30 min, washed 2x with 1 X BD Perm/Wash buffer, then incubated with Abs for 30 min. Cells were washed 2x with 1 X BD Perm/Wash buffer and resuspended in FACS buffer. Abs used include: B220 (cRA3–6B2), Bcl-2 (BCL.10C4), CD4 (GK1.5), CD8-β (YTS156.7.7), CD44 (IM7), CD45.2 (104), CD62L (H1.2F3), CD103 (2E7), CD127 (SB/199), CX_3CR1 (SA011F11), F4/80 (BM8), IFN-γ (XMG1.2), Ki67 (16A8), and KLRG1 (2F1/KLRG1) (Biolegend); CXCR3 (CXCR3–173) (BD Horizon); CD45.1 (A20) (eBioscience); CD8-α (53–6.7) (Tonbo); Cleaved Caspase-3 (D3E9) (Cell Signaling Technology); and Granzyme B (GB11) (ThermoFisher Scientific). H-$2D^b$-PA_{224} (SSLENFRAYV) and H-$2D^b$-NP_{366} (ASNENMETM) (NIH Tetramer Core Facility). Complete T cell media consisted of RPMI 1640 with 10% FBS, 4 mM L-glutamate, 0.1mM nonessential amino acids, 1 mM sodium pyruvate, 100 U/mL penicillin and streptomycin, 10 mM HEPES, and 5 mM 2-ME. OT-I cells were gated as Live/$Dead^-$, $Dump^-$ (F4/80, CD4, B220), $CD8\beta^+$, $CD45.2^-$, $CD45.1^+$.

Plasmid design & virus rescue

In-Fusion primers (Takara Bio) were designed for insertion of epitope sequences into nucleotide position 207 in the stalk of NA of influenza A/Puerto Rico/8/1934 (PR8). This site has been previously used to insert exogenous sequences without attenuation (21, 22). The SIINFEKL (N4)- AGTATAATCAACTTTGAAAAACTG, epitope or APL epitopes: SIYNFEKL (Y3)- AGTATATACAATTTTGAAAAACTG or SIITFEKL (T4) AGTATAATCACTTTTGAAAAACTG, were amplified and recombined into pDZ NA via In-Fusion HD cloning. Viruses were rescued via HEK293T transfection and amplified in embryonated chicken eggs as previously described (23). Rescued viruses were sequence confirmed and titered on Madin-Darby canine kidney (MDCK) cells (ATCC).

Cell culture and plaque assay

MDCK cells were maintained in Dulbecco's modified Eagle medium (DMEM) with 10% FBS and 1% pen-strep. Infections were carried out in infection medium PBS with 10% CaMg, 1% pen-strep, 5% bovine serum albumin) at 37°C for 1 hr. Infection medium was replaced with an agar overlay (MEM, 1 mg/mL tosyl_sulfonyl phenylalanyl chloromethlyl ketone trypsin, 1% DEAE-dextran, 5% $NaCO_3$, 2% agar), and cells were cultured at 37°C for 40 h and then fixed with 4% formaldehyde. Blocking and immunostaining were done for

1 hr at 25°C in 5% milk using the following antibodies: polyclonal anti-IAV PR8/34, 1:5,000 (V301-511-552), and peroxidase rabbit anti-chicken IgG, 1:5,000 (303-035-003; Jackson Immuno Research). TrueBlue peroxidase substrate (Kirkegard & Perry Laboratories) was used as directed for detection of virus plaques.

OT-I T cell isolation, adoptive transfer, and IAV infection

Lymph nodes were harvested from OT-I TCR-Tg CD45.1 mice and a single cell suspension was generated. The purity of $CD8^+$ $OT\text{-}I^+$ T cells was verified by flow cytometry and 50,000 or 1,000 OT-I T cells were transferred into C57Bl/6 CD45.2 mice via retro-orbital injection. For IAV infection, mice were anesthetized using a weight-based dose of ketamine/xylazine delivered intraperitoneally. Mice were infected intranasally with 40 plaque forming units (PFUs) of IAV APL viruses. During infection, all mice having weight loss exceeding 25% of their starting weight were sacrificed.

In vivo iv injection of anti-CD8 antibody and lymphocyte isolation from tissues

To discriminate parenchymal cells from blood-borne cells, mice were given an intravenous (iv) injection of anti-CD8α (3 μg) for 3 min, as described (24, 25). Mice were euthanized and spleen, lung and female reproductive tract (FRT) were harvested. Tissues were minced and washed 2x with harvest buffer (cold RPMI 1640 supplemented with 5% bovine serum, 4 mM L-glutamate and 10 mM HEPES). Lungs were incubated in a solution of RPMI 1640/ 10% bovine serum/ 2 mM $MgCl_2$/ 2mM $CaCl_2$/ 10 mM HEPES/ 4 mM L-glutamate medium containing 100 U/mL of collagenase type I (Worthington) for 45 min at 37°C. Lung pieces were then incubated in a solution of RPMI 1640/ 10% bovine serum/ 10 mM HEPES/ 4 mM L-glutamate medium containing 1.3 mM EDTA (Calbiochem) for 45 min at 37°C. FRTs were incubated in a solution of RPMI 1640/ 10% bovine serum/ 2 mM $MgCl_2$/ 2mM $CaCl_2$/ 10 mM HEPES/ 4 mM L-glutamate medium containing 50 mg/100 mL of collagenase type IV (Sigma-Aldrich) for 1 h at 37°C. Single cell suspensions of all tissues were generated and stained for flow cytometry as described above.

Tissue preparation and microscopy

C57Bl/6 mice previously infected with IAV_N4 or IAV_T4 were injected iv with anti-CD8α for three minutes prior to takedown. Lungs were fixed in 2% PFA, inflated and flash frozen in optimum cutting temperature compound. 7 μm sections were cut from each block with a Leica CM1950 cryostat and stained for imaging on a Leica DM6000B EPI fluorescent microscope (violet LED). A minimum of 500 and a maximum of 30,000 $CD45.1^+/CD8\alpha^-$ cells per section were counted using ImageJ software for a percentage of the total number of nucleated cells. Abs used were: CD8α (53–6.7) (Tonbo), CD45.1 (clone A20) (Biolegend) and donkey anti-rat (polyclonal) (Jackson ImmunoResearch).

Next generation mRNA-sequencing sample preparation.

OT-I cells from IAV_N4 and IAV_T4 infected mice were sorted and RNA was extracted using RNeasy Micro Plus kit (Qiagen). The cDNA library was prepared using strand-specific RNA-seq protocols. Samples were run on an Illumina HiSeq 2500 (50 base pair single-end). We obtained an average of 14.5 million reads per sample. Sequencing reads

were mapped to the mouse (mm10) genome using Bowtie aligner (bowtie2 version 2.3.4) with local mode, -L 22 and -N 1 parameters (26). Reads were sorted and filtered by removing the PCR duplicates with Samtools (version 1.9) (27) and assigned to Ensembl gene models (Mus_musculus.GRCm38.87.gtf) with featureCounts of the Subread software package (version 1.5) (28). Differentially expressed genes were compared between IAV_N4 and IAV_T4 samples. Statistical analysis was performed using the edgeR bioconductor package (29, 30). Multidimensional scaling was performed by with edgeR using the top 500 differentially expressed genes across samples. Sequencing data deposited under GEO series accession number GSE130609 (https://www.ncbi.nlm.nih.gov/geo/query/acc.cgi?acc=GSE130609)

Statistical analysis

GraphPad Prism was used to determine statistical significance. Student unpaired two-tailed *t* test or one-way ANOVA. A p value of < 0.05 was considered statistically significant.

RESULTS

Experimental Model

To determine how TCR signal strength impacts lung T_{RM} formation, we inserted the high affinity OT-I SIINFEKL (N4) epitope or low affinity APLs, SIYNFEKL (Y3) and SIITFEKL (T4) (20), into the stalk of neuraminidase (NA). First, we assessed whether insertion of the epitopes into the NA stalk altered the dynamics of the endogenous IAV-specific $CD8^+$ T cell response. We tracked PA_{224} and NP_{366}-specific $CD8^+$ T cells after transfer of OT-I T cells and infection with IAV epitope viruses. Prior to euthanasia, mice were injected iv with anti-CD8α antibody to distinguish between cells in vascular contiguous compartments, such as lung capillaries (antibody accessible, iv^+) and the lung parenchyma (antibody inaccessible, iv^-) (24, 25). At 10 and 34 days post infection (dpi) the number of PA_{224} and NP_{366}-specific $CD8^+$ T cells was similar between the IAV_N4 and IAV_T4 infections (Fig. S1A–D). In the lung, there was a reduction in the number of endogenous IAV-specific $CD8^+$ T cells 10 days after IAV_N4 infection, likely due to the presence of OT-I T cells and the high affinity ligand (Fig. S1A, S1B, bottom) (31). Importantly, both viruses undergo similar replication kinetics and clearance *in vivo* (Fig. S1G). These data indicate that the IAV_N4 and IAV_T4 viruses are replicating comparably and therefore any differences in OT-I T cell expansion, contraction and T_{RM} formation will not be due to alterations in engineered virus replication.

Low affinity TCR stimulation favors T_{RM} establishment

To assess how TCR signal strength impacts lung T_{RM} formation, naïve OT-I T cells were transferred into congenically distinct hosts, infected with IAV_N4, IAV_Y3 or IAV_T4, and tracked over time. As expected, at 10 dpi in the spleen and lung high affinity (N4) stimulated OT-I T cells had undergone a larger clonal burst than low affinity (Y3) or (T4) stimulated cells (Fig. 1A, 1B, S. Table 1). Reduced numbers of low affinity stimulated OT-I T cells were also observed after contraction at 34 dpi (Fig. 1C, 1D, S. Table 1). Due to differences in the clonal burst size between high and low affinity stimulated cells, we decreased the precursor number by 50x and challenged with IAV_N4 in an attempt to approximate the

effector pool observed during low affinity stimulation. At 10 dpi in the lung, the 50x reduced precursor cells had reduced expansion, albeit still at higher levels than low affinity stimulation. After contraction, we still observed greater numbers of the 50x reduced high affinity stimulated cells than low affinity stimulated cells (Fig. 1A–D, S. Table 1).

To determine the capability of differentially stimulated OT-I T cells to form lung T_{RM}, we assessed the ratio of T_{RM} cells at 34 dpi to the total lung OT-I T cells at 10 dpi in the lung (Fig. 1E). Because the clonal burst size is dramatically different between high and low affinity peptide stimulations, normalizing the number of T_{RM} cells at 34 dpi to the number of OT-I cells present in the whole lung at 10 dpi for each peptide directly compares T_{RM} formation. The OT-Is in the lung at 10 dpi represent the cells that could form T_{RM}. If TCR signal strength impacted T_{RM} formation, this ratio would be different between the high and low affinity ligands. An increased proportion of normalized OT-I T cells are present in the lung parenchyma at 34 dpi of IAV_T4 infected mice, compared to IAV_N4 infected mice and IAV_N4 infected mice with 50x reduced OT-I precursors, indicating an advantage in T_{RM} formation by lower affinity T cells (Fig. 1E). When we performed this same calculation on endogenous IAV-specific $CD8^+$ T cells, we did not observe a difference between IAV_N4 and IAV_T4 infections (Fig. S1E). As a way to resolve the ability of cells to differentiate into T_{RM}, we compared the number of lung OT-I T_{RM} cells to the total number of spleen OT-I cells at 34 dpi. A greater proportion of low affinity cells (Y3 or T4 stimulated) than high affinity stimulated cells are lung T_{RM} (Fig. 1F). There was no difference in the ratios of endogenous IAV-specific $CD8^+$ T cells (Fig. S1F). As an additional control we compared the number of splenic OT-I iv^- cells to total OT-I cells at 34 dpi as it would be expected that there would not be a difference between low and high affinity stimulation. As expected these data do not show an alteration between the different epitope viruses demonstrating the T_{RM} bias is present in non-lymphoid tissues (Fig. 1G). Importantly, reducing the precursor frequency of high affinity stimulated cells by 50x resulted in a decreased effector pool size, but still resulted in a lower ratio of T_{RM}, suggesting that the size of the effector pool alone is not altering the capacity to form T_{RM}. These data indicate that TCR signal strength can impact lung T_{RM} formation after IAV infection, where lower affinity stimulated cells may be more likely to form T_{RM}.

To alleviate technique-specific caveats (2, 32) and to determine the tissue localization we next assessed T_{RM} cells from viruses eliciting varying TCR signal strength by microscopy. Less than 5% of lung OT-I T cells from IAV_N4 or IAV_T4 infected mice were iv antibody positive. We observed increased frequencies of OT-I T cells in the lungs of IAV_N4 infected mice compared to IAV_T4 infected mice at both effector and memory time points (Fig. 2A, 2B). To determine if signal strength impacted memory formation we calculated the ratio of OT-I T cells for each ligand from 10 to 34 dpi. Similar to what we observed by flow cytometry analysis, there was an increased proportion of T4 stimulated OT-I T cells to form T_{RM} by microscopy (Fig. 2C). Together these data further support the concept that the ability to form T_{RM} is impacted by TCR signal strength.

TCR signal strength alters T_{RM} formation in a distal uninfected mucosal tissue

To determine if this was a lung-specific phenotype, we assessed T_{RM} formation in a distal uninfected tissue, the female reproductive tract (FRT), which would lack antigen and inflammation from the IAV infection. Equivalent numbers of endogenous IAV-specific $CD8^+$ T cells were detected in the FRT after IAV_N4 or IAV_T4 infections (Fig. 3A, 3B). Consistent with the spleen and lung, increased numbers of OT-I T cells were present in the FRT after IAV_N4 infection, when compared to IAV_T4 infection (Fig. 3C, 3D). Again, we compared the ratio of T_{RM} cells in the FRT at 34 dpi to the total T_{RM} precursors at 10 dpi which demonstrated an increased proportion of T_{RM} cells generated after IAV_T4 infection (Fig. 3E). These data are consistent with the concept that T_{RM} formation is impacted by the strength of antigen-specific stimulation.

TCR signal strength does not impact survival, apoptosis or proliferation during contraction

To understand the disparity in T_{RM} formation between high and low affinity stimulated cells, we analyzed these cells early during contraction at 15dpi. Similar to 10 and 34 dpi, greater numbers of OT-I T cells were present after IAV_N4 challenge at 15 dpi (Fig. S2A). We assessed the expression of Ki67 (proliferation), cleaved caspase-3 (apoptosis) and Bcl-2 (prosurvival molecule) in IAV_N4 or IAV_T4 primed OT-I T cells. Equal expression of Ki67, cleaved caspase-3 and Bcl-2 was seen (Fig. S2B,C). These data suggest, at least at this time point, that alteration in T_{RM} between cells with low and high TCR stimulation is not due to alterations in contraction.

Strength of TCR simulation correlates with T cell differentiation status

Memory $CD8^+$ T cell differentiation is shaped by the strength of TCR stimulation, where higher affinity interaction correlates with greater T_{EM} generation over T_{CM} generation (17), elevated KLRG1 expression, reduced CD127 (IL-7Rα) expression (33, 34), and increased CX_3CR1 expression (35, 36). We assessed these correlations in our IAV model and determined the T_{CM}/T_{EM} ratio of OT-I T cells in the spleen after IAV_N4 or IAV_T4 infections. At 34 dpi, N4 stimulated OT-I T cells had an increased percentage of T_{EM} cells when compared to low affinity stimulated OT-I cells (Fig. 4A, 4B). At 10 dpi in the spleen, an increased frequency of high affinity stimulated OT-I T cells expressed KLRG1 (Fig. 4C, 4D). In both the spleen and lung, a greater percentage of low affinity stimulated OT-I T cells expressed CD127 (Fig. 4C, 4D). This trend was maintained in the lung at 34 dpi (Fig. 4E, 4F). Additionally, we observed a greater frequency of low affinity stimulated cells expressing no or intermediate levels of CX_3CR1 in the spleen (Fig. 4G, 4H). Consistent with published results, the majority of lung T_{RM} cells are CX_3CR1^{neg} (Fig. 4G, 4H) (35), and the low and high affinity stimulated cells expressed equivalent amounts of CX_3CR1 (Fig. 4G, 4H). Overall, our data are consistent with previous reports where high affinity stimulated cells form more T_{EM} than T_{CM}, express more KLRG1 and less CD127, and express higher amounts of CX_3CR1 (17, 33–36). These data are consistent with the idea that high affinity stimulated cells are more differentiated towards an effector fate than low affinity stimulated cells, with negative consequence for T_{RM} cell differentiation.

Lung T_{RM} cell phenotype is independent of TCR signal strength

CD103, which binds to E-cadherin promoting residency and CD69, which antagonizes S1PR1 preventing tissue egress, have been classically used as markers for T_{RM} (37). To determine the heterogeneity of cells in the lungs after high and low TCR stimulation, we assessed CD103 and CD69 expression on iv^- OT-I T cells on 10 and 34 dpi. At 10 dpi, approximately 50% of iv^- OT-I T cells had upregulated CD103 in the lung, with or without CD69 expression, regardless of TCR affinity stimulation (Fig. 5A, 5B). At 34 dpi, the frequency of $CD103^+$ OT-I T cells in the tissue increased to approximately 75%, regardless of the TCR ligand affinity (Fig. 5A, 5B). The majority of $CD103^+$ cells were also $CD69^+$ (Fig. 5A, 5B). At both 10 and 34 dpi we observed slightly more low affinity $CD103^-$ $CD69^-$ cells in the lung. We also assessed CD103 and CD69 expression of iv^- OT-I T cells in the FRT. At 10 dpi more low affinity cells were $CD103^+$ $CD69^+$ and $CD103^-$ $CD69^+$, but by 34 dpi, low and high affinity cells were expressing similar levels with the majority of cells expressing $CD103^-$ $CD69^+$ (Fig. 5A, 5B) These data indicate that T_{RM} expression of CD103 and CD69 in the lung is independent of TCR affinity.

Production of IFN-γ has been demonstrated to be a critical mediator of the sensing and alarm function of T_{RM} to rapidly protect tissues from reinfection (38, 39). The ability of lung T_{RM} cells generated by high or low TCR affinity stimulation to produce IFN-γ was not impacted as measured by *ex vivo* stimulation with the high affinity N4 peptide (Fig. 5C, 5D). OT-I memory cells in the spleen also produced equal amounts of IFN-γ after stimulation (Fig. 5E, 5F). We also assessed granzyme B production by lung T_{RM}s. Similar to IFN-γ, granzyme B production was equivalent between low and high affinity primed cells (Fig. S3A–B). We also assessed IFN-γ and granzyme B expression in the spleen at 10 dpi and observed equal amounts between low and high affinity primed cells after stimulation (Fig. S3C–F).

To determine functional dynamics of activation *ex vivo* we stimulated OT-Is from IAV_N4 or IAV_T4 primed mice with two concentrations of either N4 or T4 peptide. Low affinity primed cells stimulated *ex vivo* with a 10-fold reduced concentration of N4 peptide produced less IFN-γ (Fig. S3G). Additionally, even with low affinity T4 peptide restimulation, high and low affinity primed cells produced equivalent IFN-γ at high peptide concentration (Fig. S3G). These data demonstrate that low affinity TCR interactions during a primary immune response does not alter the functionality of T_{RM} cells upon restimulation, as measured by IFN-γ and granzyme B. Together these data indicate that TCR signal strength does not alter markers of residency in the lung or the response of T_{RM} cells to stimulation.

T_{RM} longevity is independent of TCR affinity

After IAV infection, the number of lung T_{RM} cells and protection against secondary infection wanes with time (4, 5). To determine if T_{RM} maintenance in the lung is impacted by varying TCR signal strength, we assessed the number of OT-I T_{RM} cells at late memory time points after IAV_N4 or IAV_T4 infection. From 34 to 133 dpi, the number of both high and low affinity stimulated OT-I T_{RM} cells decreased at a similar rate in the lung and FRT **(**Fig. 6A and C). Memory was maintained in the spleen regardless of TCR affinity (Fig. 6B).

These data suggest that while TCR signal strength impacts T_{RM} formation it does not alter the longevity of these cells in the tissues, therefore cell extrinsic factors may be critical for long-term maintenance within the lung.

Distinct transcriptomes of high and low affinity lung T_{RM} cells

To determine the potential transcriptional signatures leading to increased T_{RM} during low affinity stimulation we sorted OT-I T_{RM} from the lungs of IAV_N4 or IAV_T4 infected mice and performed RNA-seq. Multidimensional scaling demonstrates alterations in the transcriptomes of low and high affinity stimulated cells. Importantly there were no major differences if 50x lower numbers of OT-I were transferred for IAV_N4 stimulation. These data suggest that TCR stimulation and not clonal burst size are responsible for the majority of the transcriptional changes. There were 816 differentially expressed genes between IAV_N4 and IAV_T4 stimulation (FDR < 0.05) (Fig. 7A). Interestingly, several genes involved cell survival were increased in low affinity stimulated cells (Il2ra, Bcl2, Sema6d, Ifitm3) (Fig. 7B). Additionally, there was increased expression of genes that may promote residency (*e.g.* Ccr8 a marker of residency for T_{RM} in the skin (40) and Itih5 which blocks tumor metastases (41, 42)). Conversely, high affinity stimulated cells exhibited increased cell death and activation markers (Casp9, Cd5, Ctla4, and Cd27) (Fig. 7B). Together these data demonstrate that low affinity stimulation drives a transcriptional program that enhances the potential to survive in the lung tissues.

DISCUSSION

In this study, we assessed the ability of TCR signal strength to regulate lung T_{RM} formation. We inserted N4 peptide or lower affinity APLs, Y3 and T4, into IAV to assess T_{RM} formation, heterogeneity, response to stimulation and maintenance over time. We analyzed T_{RM} formation by using two independent readouts, flow cytometry and microscopy, to alleviate technique-specific caveats (2, 32). We discovered that lower affinity TCR stimulation elicits a bias towards T_{RM} formation in the lung after IAV infection. Interestingly this low affinity bias was also observed in a distal uninfected mucosal tissue. Lower TCR stimulation drove a distinct transcriptional profile in T_{RM} within the lungs resulting increased expression of pro-survival genes. Additionally, TCR signal strength impacted the differentiation of memory cells, where high affinity stimulated cells formed more T_{EM} cells and expressed greater levels of KLRG1 and CX_3CR1 than low affinity stimulated cells, consistent with previous studies (17, 33–36). However, there was no impact of TCR affinity on the expression of T_{RM} markers, or the response of T_{RM} to stimulation, suggesting that T_{RM} quality was not altered. T_{RM} in the lung are short lived, which negatively impacts protection over time (3–6). Importantly, the maintenance of T_{RM} was not impacted by TCR signal strength. Interestingly, in humans IAV-specific memory $CD8^+$ T cells of different clones reacting to the same antigen have different ratios of T_{RM} formation in the lung suggesting the possibility that a range of TCR signal strength can differentially drive T_{RM} in people (43). In conclusion, we demonstrated that T cell intrinsic factors can impact T_{RM} as increased TCR signal strength is negatively correlated with T_{RM} formation. These findings have implications for vaccine design and T cell-based cancer therapeutics by

suggesting that excessive T cell stimulation may bias the population away from T_{RM} differentiation.

We chose to use a fixed TCR and alter the affinity of the peptide in the context of IAV infection to study T_{RM} formation in the lung. This system allowed us to transfer in a known number of antigen-specific cells that are easily trackable during all stages of the immune response by both flow cytometry and microscopy. IAV_N4 and IAV_T4 viruses replicated equivalently, ensuring that the OT-I T cells were present in a lung environment with equivalent viral load, antigen load, length of antigen presentation and access to the same populations of antigen presenting cells. Importantly, the presence of endogenous $CD8^+$ T cells does not alter the response of OT-I T cells to low affinity antigens (20). Additionally, all peptides used in this study bind equivalently to the same MHC-I, H-$2K^b$, thereby eliminating a potential caveat (20). Together this reductionist system allowed us to specifically assess the role of TCR signal strength, eliminating many of the potentially confounding variables found using endogenous epitopes and polyclonal T cell responses. Therefore, we were able to conclude that T_{RM} formation is at least partially influenced by TCR affinity. However, the presence of a large precursor number can alter the ability of stimulated $CD8^+$ T cells to form memory (44). To ensure that a large effector population was not solely responsible we decreased the precursor frequency by 50x to reduce the clonal burst size. Reduced precursor cells stimulated with high affinity antigen were still less effective at forming T_{RM} than low affinity stimulated cells and had similar transcriptional profiles to high affinity cells with a larger number of precursors. These data further suggest that strength of TCR negatively correlates with the capacity to form T_{RM}.

The environment is a critical driver of T_{RM} formation in NLTs. Signals that drive T_{RM} can be expressed in the steady state, and can be enhanced or induced by virus infection. While extracellular queues are required for T_{RM} formation, presence of antigen within the tissue is unclear. Previous studies have demonstrated that depending on the tissue, infection, and site of replication antigen can either be required or dispensable for establishment of T_{RM} (45–50). Non-specific inflammation can pull $CD8^+$ T cells into a NLT which then become resident (48, 49). In contrast, non-pulmonary antigen delivery in the context of lung inflammation does not induce lung T_{RM} (14). Additionally, the presence of cognate antigen in the lung is necessary for optimal sustained expression of CD103 and CD69 by T_{RM} precursors (14). This is analogous with the antigen two hit model for effector T cell function and survival within the lung (51, 52). Conversely, T_{RM} formation after IAV infection occurred in the FRT in the absence of local antigen or inflammation, suggesting that TCR signaling during priming in secondary lymphoid organs imprints memory differentiation including T_{RM} formation. This further highlights the importance of TCR signal strength during priming. It is interesting to speculate on the different requirements of residency in various mucosal tissues. Some may simply be due to tissue-specific factors, such as what cell types are present and the basal production of cytokines and chemokines. This is further supported by the distinct transcriptional profiles of T_{RM} from the lung, skin and gut (10). The plasticity of T_{RM} formation in diverse NLTs ensures adequate responses at the site of a local infection.

During IAV infections $CD8^+$ memory responses are impacted by the dynamics of antigen presentation. Stimulation of IAV-specific $CD8^+$ T cells by different immunodominant epitopes result in differential expression of CD103 and CD69, and differentially regulated transcriptomes in T_{RM} cells (53). This could be driven by multiple factors including antigen load, TCR avidity and the APC subset presenting antigen. $CD8^+$ T cells bind to H-$2D^b$-PA_{224} with higher avidity than H-$2D^b$-NP_{366} leading to greater IFN-γ *ex vivo* (54). In contrast, OT-I T_{RM} cells generated from both high and low affinity antigen can produce equivalent amounts of IFN-γ *ex vivo*. These epitope-specific differences could be driven by several factors. Not all cells can present NP_{336} and PA_{224} epitopes after IAV infection, and the levels of antigen presentation for each epitope varies (15, 55). Furthermore, antigen abundance can dictate levels of memory and T_{RM} during IAV infection (6, 55). Together these data suggest that in addition to environment, the antigen load, TCR avidity, and APC subset all can also affect lung T_{RM} formation. Our system bypasses antigen load and APC subset by expressing the low and high affinity epitopes off of the same IAV gene segment, allowing for direct assessment of the role of TCR signaling in T_{RM} ontogeny. Using this reductionist approach, we identified distinct transcriptional signatures between low and high affinity stimulated T_{RM}s. Interestingly several of the genes increased in the low affinity cells are involved in cellular survival and may underpin the enhanced ability to form T_{RM}. Sema6d is involved in stabilizing CD127 surface expression on memory $CD4^+$ T cells (56). Differences were also seen Ifitm3 which may help low affinity cells survive reinfection and help to prevent the possibility of pathogen escape by having a diverse array of T_{RM}s in the lung (57, 58). We also identified increased expression of Itih5, an inter-alpha trypsin inhibitor, which is involved in extracellular matrix stabilization and prevention of tumor metastases (41, 42, 59). Together these data suggest that transcriptional changes that promote survival and retention in the tissue may be responsible for increased capacity of lower affinity stimulated cells to form T_{RM}.

Using a reductionist approach, we were able to demonstrate T cell intrinsic properties can impact the differentiation of T_{RM} cells during an acute viral infection. Lower affinity stimulation leads to increased proportion of cells capable of forming T_{RM}. While higher affinity stimulations induce larger clonal burst sizes leading to a greater total number of T_{RM} cells, having a bias in T_{RM} formation for lower affinity cells helps to ensure a broad diversity in the T_{RM} pool. This may be critical in preventing escape from $CD8^+$ T cell-mediated pathogen control upon reinfection.

Supplementary Material

Refer to Web version on PubMed Central for supplementary material.

ACKNOWLEDGEMENTS

We thank Dr. Steve Jameson for helpful discussions regarding this project and Dr. Vaiva Vezys for the gift of $CD45.1^+$ OT-I mice. We acknowledge the NIH Tetramer Core Facility for providing H-$2D^b$-PA_{224} and H-$2D^b$-NP_{366} tetramers. We also thank the UMN Flow Cytometry Resource Facility, Genomics Center, and University Imaging Center for expert technical assistance, especially Dr. Jason Mitchell.

GRANT SUPPORT

This work was supported by NIH K22 AI110581 and NIH R01 AI132962 to RAL. JKF was supported by T32 HL007741 and EJF by T32 AI007313. This project was also funded in part with Federal funds from NIAID, NIH and the department of Health and Human Services, under CEIRS Contract No. HHSN272201400005C.

REFERENCES

1. Sallusto F, Lenig D, Forster R, Lipp M, and Lanzavecchia A. 1999 Two subsets of memory T lymphocytes with distinct homing potentials and effector functions. Nature 401: 708–712. [PubMed: 10537110]
2. Schenkel JM, and Masopust D. 2014 Tissue-resident memory T cells. Immunity 41: 886–897. [PubMed: 25526304]
3. Hogan RJ, Usherwood EJ, Zhong W, Roberts AA, Dutton RW, Harmsen AG, and Woodland DL. 2001 Activated antigen-specific CD8+ T cells persist in the lungs following recovery from respiratory virus infections. J Immunol 166: 1813–1822. [PubMed: 11160228]
4. Wu T, Hu Y, Lee YT, Bouchard KR, Benechet A, Khanna K, and Cauley LS. 2014 Lung-resident memory CD8 T cells (TRM) are indispensable for optimal cross-protection against pulmonary virus infection. J Leukoc Biol 95: 215–224. [PubMed: 24006506]
5. Slutter B, Van Braeckel-Budimir N, Abboud G, Varga SM, Salek-Ardakani S, and Harty JT. 2017 Dynamics of influenza-induced lung-resident memory T cells underlie waning heterosubtypic immunity. Sci Immunol 2.
6. Pizzolla A, Nguyen THO, Smith JM, Brooks AG, Kedzieska K, Heath WR, Reading PC, and Wakim LM. 2017 Resident memory CD8(+) T cells in the upper respiratory tract prevent pulmonary influenza virus infection. Sci Immunol 2.
7. Masopust D, Vezys V, Marzo AL, and Lefrancois L. 2001 Preferential localization of effector memory cells in nonlymphoid tissue. Science 291: 2413–2417. [PubMed: 11264538]
8. Gebhardt T, Wakim LM, Eidsmo L, Reading PC, Heath WR, and Carbone FR. 2009 Memory T cells in nonlymphoid tissue that provide enhanced local immunity during infection with herpes simplex virus. Nat Immunol 10: 524–530. [PubMed: 19305395]
9. Jiang X, Clark RA, Liu L, Wagers AJ, Fuhlbrigge RC, and Kupper TS. 2012 Skin infection generates non-migratory memory CD8+ T(RM) cells providing global skin immunity. Nature 483: 227–231. [PubMed: 22388819]
10. Mackay LK, Rahimpour A, Ma JZ, Collins N, Stock AT, Hafon ML, Vega-Ramos J, Lauzurica P, Mueller SN, Stefanovic T, Tscharke DC, Heath WR, Inouye M, Carbone FR, and Gebhardt T. 2013 The developmental pathway for CD103(+)CD8+ tissue-resident memory T cells of skin. Nat Immunol 14: 1294–1301. [PubMed: 24162776]
11. Le Goffic R, Arshad MI, Rauch M, L'Helgoualc'h A, Delmas B, Piquet-Pellorce C, and Samson M. 2011 Infection with influenza virus induces IL-33 in murine lungs. Am J Respir Cell Mol Biol 45: 1125–1132. [PubMed: 21642589]
12. DeBerge MP, Ely KH, and Enelow RI. 2014 Soluble, but not transmembrane, TNF-alpha is required during influenza infection to limit the magnitude of immune responses and the extent of immunopathology. J Immunol 192: 5839–5851. [PubMed: 24790150]
13. Takamura S, Yagi H, Hakata Y, Motozono C, McMaster SR, Masumoto T, Fujisawa M, Chikaishi T, Komeda J, Itoh J, Umemura M, Kyusai A, Tomura M, Nakayama T, Woodland DL, Kohlmeier JE, and Miyazawa M. 2016 Specific niches for lung-resident memory CD8+ T cells at the site of tissue regeneration enable CD69-independent maintenance. The Journal of experimental medicine 213: 3057–3073. [PubMed: 27815325]
14. McMaster SR, Wein AN, Dunbar PR, Hayward SL, Cartwright EK, Denning TL, and Kohlmeier JE. 2018 Pulmonary antigen encounter regulates the establishment of tissue-resident CD8 memory T cells in the lung airways and parenchyma. Mucosal Immunol.
15. Ballesteros-Tato A, Leon B, Lee BO, Lund FE, and Randall TD. 2014 Epitope-specific regulation of memory programming by differential duration of antigen presentation to influenza-specific CD8(+) T cells. Immunity 41: 127–140. [PubMed: 25035957]
16. Iborra S, Martinez-Lopez M, Khouili SC, Enamorado M, Cueto FJ, Conde-Garrosa R, Del Fresno C, and Sancho D. 2016 Optimal Generation of Tissue-Resident but Not Circulating Memory T

Cells during Viral Infection Requires Crosspriming by DNGR-1(+) Dendritic Cells. Immunity 45: 847–860. [PubMed: 27692611]

17. Smith-Garvin JE, Burns JC, Gohil M, Zou T, Kim JS, Maltzman JS, Wherry EJ, Koretzky GA, and Jordan MS. 2010 T-cell receptor signals direct the composition and function of the memory CD8+ T-cell pool. Blood 116: 5548–5559. [PubMed: 20847203]
18. Maru S, Jin G, Schell TD, and Lukacher AE. 2017 TCR stimulation strength is inversely associated with establishment of functional brain-resident memory CD8 T cells during persistent viral infection. PLoS Pathog 13: e1006318. [PubMed: 28410427]
19. Frost EL, Kersh AE, Evavold BD, and Lukacher AE. 2015 Cutting Edge: Resident Memory CD8 T Cells Express High-Affinity TCRs. J Immunol 195: 3520–3524. [PubMed: 26371252]
20. Zehn D, Lee SY, and Bevan MJ. 2009 Complete but curtailed T-cell response to very low-affinity antigen. Nature 458: 211–214. [PubMed: 19182777]
21. Heaton NS, Sachs D, Chen CJ, Hai R, and Palese P. 2013 Genome-wide mutagenesis of influenza virus reveals unique plasticity of the hemagglutinin and NS1 proteins. Proc Natl Acad Sci U S A 110: 20248–20253. [PubMed: 24277853]
22. Schmidt ME, Knudson CJ, Hartwig SM, Pewe LL, Meyerholz DK, Langlois RA, Harty JT, and Varga SM. 2018 Memory CD8 T cells mediate severe immunopathology following respiratory syncytial virus infection. PLoS pathogens 14: e1006810. [PubMed: 29293660]
23. Langlois RA, Varble A, Chua MA, Garcia-Sastre A, and tenOever BR. 2012 Hematopoietic-specific targeting of influenza A virus reveals replication requirements for induction of antiviral immune responses. Proceedings of the National Academy of Sciences of the United States of America 109: 12117–12122. [PubMed: 22778433]
24. Galkina E, Thatte J, Dabak V, Williams MB, Ley K, and Braciale TJ. 2005 Preferential migration of effector CD8+ T cells into the interstitium of the normal lung. J Clin Invest 115: 3473–3483. [PubMed: 16308575]
25. Anderson KG, Mayer-Barber K, Sung H, Beura L, James BR, Taylor JJ, Qunaj L, Griffith TS, Vezys V, Barber DL, and Masopust D. 2014 Intravascular staining for discrimination of vascular and tissue leukocytes. Nat Protoc 9: 209–222. [PubMed: 24385150]
26. Langmead B, and Salzberg SL. 2012 Fast gapped-read alignment with Bowtie 2. Nat Methods 9: 357–359. [PubMed: 22388286]
27. Li H, Handsaker B, Wysoker A, Fennell T, Ruan J, Homer N, Marth G, Abecasis G, Durbin R, and Genome S Project Data Processing. 2009. The Sequence Alignment/Map format and SAMtools. Bioinformatics 25: 2078–2079. [PubMed: 19505943]
28. Liao Y, Smyth GK, and Shi W. 2014 featureCounts: an efficient general purpose program for assigning sequence reads to genomic features. Bioinformatics 30: 923–930. [PubMed: 24227677]
29. Robinson MD, McCarthy DJ, and Smyth GK. 2010 edgeR: a Bioconductor package for differential expression analysis of digital gene expression data. Bioinformatics 26: 139–140. [PubMed: 19910308]
30. McCarthy DJ, Chen Y, and Smyth GK. 2012 Differential expression analysis of multifactor RNA-Seq experiments with respect to biological variation. Nucleic Acids Res 40: 4288–4297. [PubMed: 22287627]
31. Jenkins MR, Webby R, Doherty PC, and Turner SJ. 2006 Addition of a prominent epitope affects influenza A virus-specific CD8+ T cell immunodominance hierarchies when antigen is limiting. J Immunol 177: 2917–2925. [PubMed: 16920927]
32. Steinert EM, Schenkel JM, Fraser KA, Beura LK, Manlove LS, Igyarto BZ, Southern PJ, and Masopust D. 2015 Quantifying Memory CD8 T Cells Reveals Regionalization of Immunosurveillance. Cell 161: 737–749. [PubMed: 25957682]
33. Joshi NS, Cui W, Chandele A, Lee HK, Urso DR, Hagman J, Gapin L, and Kaech SM. 2007 Inflammation directs memory precursor and short-lived effector CD8(+) T cell fates via the graded expression of T-bet transcription factor. Immunity 27: 281–295. [PubMed: 17723218]
34. Kaech SM, Tan JT, Wherry EJ, Konieczny BT, Surh CD, and Ahmed R. 2003 Selective expression of the interleukin 7 receptor identifies effector CD8 T cells that give rise to long-lived memory cells. Nat Immunol 4: 1191–1198. [PubMed: 14625547]

35. Gerlach C, Moseman EA, Loughhead SM, Alvarez D, Zwijnenburg AJ, Waanders L, Garg R, de la Torre JC, and von Andrian UH. 2016 The Chemokine Receptor CX3CR1 Defines Three Antigen-Experienced CD8 T Cell Subsets with Distinct Roles in Immune Surveillance and Homeostasis. Immunity 45: 1270–1284. [PubMed: 27939671]
36. Bottcher JP, Beyer M, Meissner F, Abdullah Z, Sander J, Hochst B, Eickhoff S, Rieckmann JC, Russo C, Bauer T, Flecken T, Giesen D, Engel D, Jung S, Busch DH, Protzer U, Thimme R, Mann M, Kurts C, Schultze JL, Kastenmuller W, and Knolle PA. 2015 Functional classification of memory CD8(+) T cells by CX3CR1 expression. Nat Commun 6: 8306. [PubMed: 26404698]
37. Masopust D, and Soerens AG. 2019 Tissue-Resident T Cells and Other Resident Leukocytes. Annu Rev Immunol 37: 521–546. [PubMed: 30726153]
38. Schenkel JM, Fraser KA, Beura LK, Pauken KE, Vezys V, and Masopust D. 2014 T cell memory. Resident memory CD8 T cells trigger protective innate and adaptive immune responses. Science 346: 98–101. [PubMed: 25170049]
39. Schenkel JM, Fraser KA, Vezys V, and Masopust D. 2013 Sensing and alarm function of resident memory CD8(+) T cells. Nat Immunol 14: 509–513. [PubMed: 23542740]
40. McCully ML, Ladell K, Andrews R, Jones RE, Miners KL, Roger L, Baird DM, Cameron MJ, Jessop ZM, Whitaker IS, Davies EL, Price DA, and Moser B. 2018 CCR8 Expression Defines Tissue-Resident Memory T Cells in Human Skin. J Immunol 200: 1639–1650. [PubMed: 29427415]
41. Veeck J, Chorovicer M, Naami A, Breuer E, Zafrakas M, Bektas N, Durst M, Kristiansen G, Wild PJ, Hartmann A, Knuechel R, and Dahl E. 2008 The extracellular matrix protein ITIH5 is a novel prognostic marker in invasive node-negative breast cancer and its aberrant expression is caused by promoter hypermethylation. Oncogene 27: 865–876. [PubMed: 17653090]
42. Sasaki K, Kurahara H, Young ED, Natsugoe S, Ijichi A, Iwakuma T, and Welch DR. 2017 Genome-wide in vivo RNAi screen identifies ITIH5 as a metastasis suppressor in pancreatic cancer. Clin Exp Metastasis 34: 229–239. [PubMed: 28289921]
43. Pizzolla A, Nguyen TH, Sant S, Jaffar J, Loudovaris T, Mannering SI, Thomas PG, Westall GP, Kedzierska K, and Wakim LM. 2018 Influenza-specific lung-resident memory T cells are proliferative and polyfunctional and maintain diverse TCR profiles. J Clin Invest 128: 721–733. [PubMed: 29309047]
44. Badovinac VP, Haring JS, and Harty JT. 2007 Initial T cell receptor transgenic cell precursor frequency dictates critical aspects of the CD8(+) T cell response to infection. Immunity 26: 827–841. [PubMed: 17555991]
45. McMaster SR, Wilson JJ, Wang H, and Kohlmeier JE. 2015 Airway-Resident Memory CD8 T Cells Provide Antigen-Specific Protection against Respiratory Virus Challenge through Rapid IFN-gamma Production. J Immunol 195: 203–209. [PubMed: 26026054]
46. Muschaweckh A, Buchholz VR, Fellenzer A, Hessel C, Konig PA, Tao S, Tao R, Heikenwalder M, Busch DH, Korn T, Kastenmuller W, Drexler I, and Gasteiger G. 2016 Antigen-dependent competition shapes the local repertoire of tissue-resident memory CD8+ T cells. The Journal of experimental medicine 213: 3075–3086. [PubMed: 27899444]
47. Khan TN, Mooster JL, Kilgore AM, Osborn JF, and Nolz JC. 2016 Local antigen in nonlymphoid tissue promotes resident memory CD8+ T cell formation during viral infection. The Journal of experimental medicine 213: 951–966. [PubMed: 27217536]
48. Mackay LK, Stock AT, Ma JZ, Jones CM, Kent SJ, Mueller SN, Heath WR, Carbone FR, and Gebhardt T. 2012 Long-lived epithelial immunity by tissue-resident memory T (TRM) cells in the absence of persisting local antigen presentation. Proceedings of the National Academy of Sciences of the United States of America 109: 7037–7042. [PubMed: 22509047]
49. Shin H, and Iwasaki A. 2012 A vaccine strategy that protects against genital herpes by establishing local memory T cells. Nature 491: 463–467. [PubMed: 23075848]
50. Turner DL, Bickham KL, Thome JJ, Kim CY, D'Ovidio F, Wherry EJ, and Farber DL. 2014 Lung niches for the generation and maintenance of tissue-resident memory T cells. Mucosal Immunol 7: 501–510. [PubMed: 24064670]

51. McGill J, Van Rooijen N, and Legge KL. 2008 Protective influenza-specific CD8 T cell responses require interactions with dendritic cells in the lungs. The Journal of experimental medicine 205: 1635–1646. [PubMed: 18591411]

52. McGill J, Van Rooijen N, and Legge KL. 2010 IL-15 trans-presentation by pulmonary dendritic cells promotes effector CD8 T cell survival during influenza virus infection. J Exp Med 207: 521–534. [PubMed: 20212069]

53. Yoshizawa A, Bi K, Keskin DB, Zhang G, Reinhold B, and Reinherz EL. 2018 TCR-pMHC encounter differentially regulates transcriptomes of tissue-resident CD8 T cells. Eur J Immunol 48: 128–150. [PubMed: 28872670]

54. La Gruta NL, Turner SJ, and Doherty PC. 2004 Hierarchies in cytokine expression profiles for acute and resolving influenza virus-specific CD8+ T cell responses: correlation of cytokine profile and TCR avidity. J Immunol 172: 5553–5560. [PubMed: 15100298]

55. La Gruta NL, Kedzierska K, Pang K, Webby R, Davenport M, Chen W, Turner SJ, and Doherty PC. 2006 A virus-specific CD8+ T cell immunodominance hierarchy determined by antigen dose and precursor frequencies. Proceedings of the National Academy of Sciences of the United States of America 103: 994–999. [PubMed: 16418289]

56. O'Connor BP, Eun SY, Ye Z, Zozulya AL, Lich JD, Moore CB, Iocca HA, Roney KE, Holl EK, Wu QP, van Deventer HW, Fabry Z, and Ting JP. 2008 Semaphorin 6D regulates the late phase of CD4+ T cell primary immune responses. Proceedings of the National Academy of Sciences of the United States of America 105: 13015–13020. [PubMed: 18728195]

57. Allen EK, Randolph AG, Bhangale T, Dogra P, Ohlson M, Oshansky CM, Zamora AE, Shannon JP, Finkelstein D, Dressen A, DeVincenzo J, Caniza M, Youngblood B, Rosenberger CM, and Thomas PG. 2017 SNP-mediated disruption of CTCF binding at the IFITM3 promoter is associated with risk of severe influenza in humans. Nat Med 23: 975–983. [PubMed: 28714988]

58. Wakim LM, Gupta N, Mintern JD, and Villadangos JA. 2013 Enhanced survival of lung tissue-resident memory CD8(+) T cells during infection with influenza virus due to selective expression of IFITM3. Nat Immunol 14: 238–245. [PubMed: 23354485]

59. Chen L, Mao SJ, McLean LR, Powers RW, and Larsen WJ. 1994 Proteins of the inter-alpha-trypsin inhibitor family stabilize the cumulus extracellular matrix through their direct binding with hyaluronic acid. J Biol Chem 269: 28282–28287. [PubMed: 7525572]

KEY POINTS

1. Low affinity stimulated $CD8^+$ T cells have an advantage in forming T_{RM}.
2. High and low affinity stimulated T_{RM}s have distinct transcriptomes.
3. T_{RM} longevity is not impacted by strength of TCR stimulation.

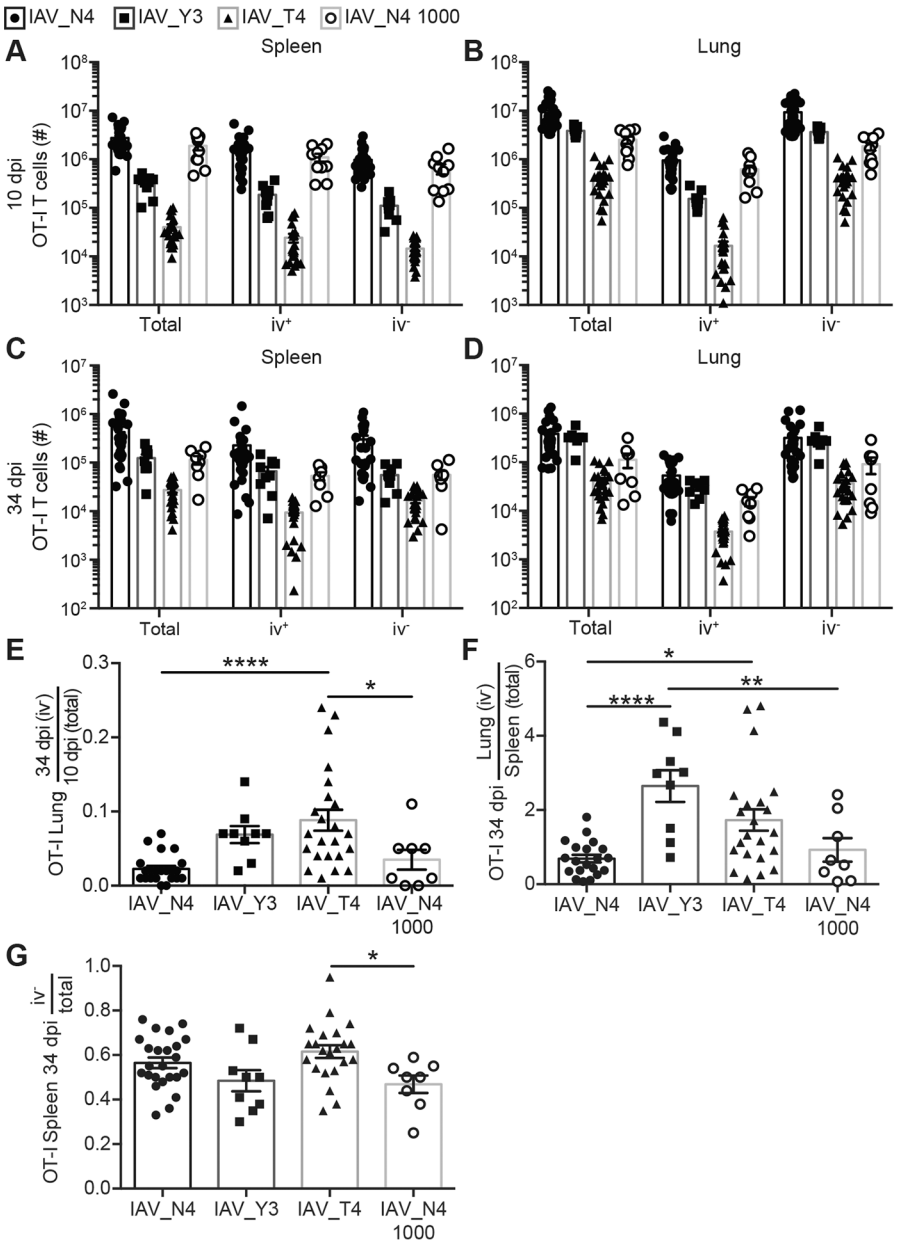

Figure 1. CD8$^+$ T cells stimulated with high or low affinity ligands can form lung T_{RM}.

CD45.1$^+$ OT-I T cells were transferred into CD45.2$^+$ hosts and were infected with 40 PFU of IAV_N4, IAV_Y3 or IAV_T4. Spleen and lungs were harvested after anti-CD8α iv injections. (**A-D**) The number of OT-I T cells, either total (iv$^+$ and iv$^-$ combined), iv$^+$, or iv$^-$ cells in the spleen (**A, C**) and lung (**B, D**) from mice infected IAV_N4, IAV_Y3, IAV_T4, or IAV_N4 with 1000 OT-I precursors at 10 (**A, B**) or 34 (**C, D**) dpi. (**E**) The number of iv$^-$ OT-I T cells in the lung at 34 dpi was divided by the average number of total OT-I T cells in the lung at 10 dpi. (**F**) The number of iv$^-$ OT-I T cells in the lung at 34 dpi was divided by the number of total OT-I T cells in the spleen at 34 dpi, for each mouse. (**G**) The number of iv$^-$ OT-I T cells in the spleen at 34 dpi was divided by the number of total OT-I T cells in the spleen at 34 dpi, for each mouse. The results are compiled from at 2–5 independent

experiments with at least 4 mice per group, per experiment (± SEM). **A-D** one-way ANOVA (see table S1). **E-G** *$p < 0.05$, ** $p < 0.01$, *** $p < 0.001$, **** $p < 0.0001$ (unpaired t test).

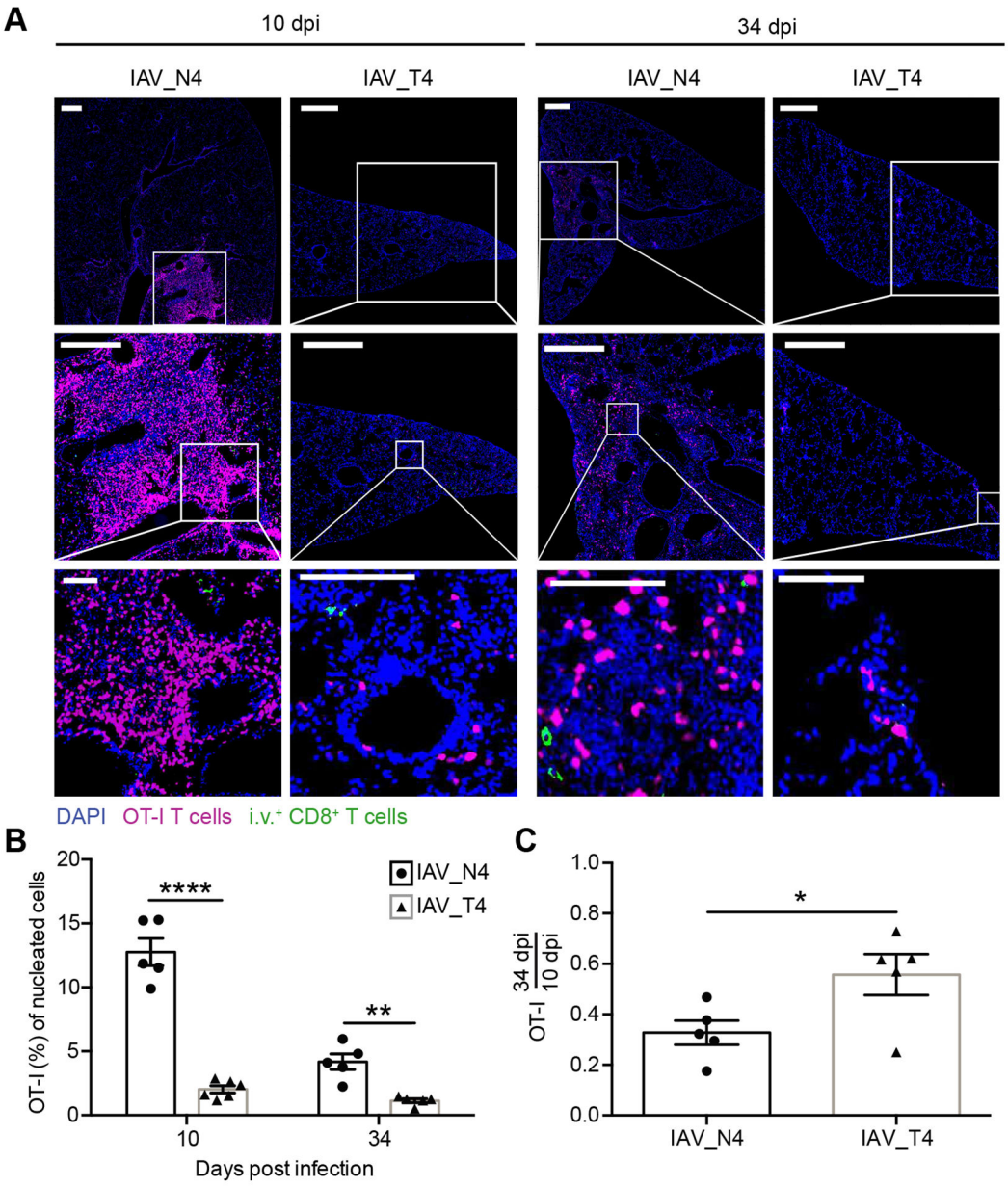

Figure 2. Confirmation of T_{RM} formation by $CD8^+$ T cells stimulated with high or low affinity peptides by microscopy.

Challenged mice were generated as in Figure 1. Tissue sections were stained for DAPI (blue), CD45.1 (magenta) and donkey anti-rat (green) to identify nucleated cells, OT-I T cells and iv^+ cells, respectively. (**A**) Representative images of lungs from IAV_N4 or IAV_T4 epitopes at 10 or 34 dpi. White bars = 500 μm for top and middle rows, 100 μm for bottom row. (**B**) The percentage of OT-I T cells ($CD45.1^+$) of nucleated cells (DAPI) in the lung from IAV_N4 or IAV_T4 infected mice. Each point represents a mouse, from two distinct lung sections, which were taken at least 100 μm apart. (**C**) The percentage of OT-I T cells in the lung at 34 dpi was divided by the average number of OT-I T cells in the lung at 10 dpi for each infection. The results (**B, C**) are compiled from 2 independent experiments

with 2–3 mice per group, per experiment (± SEM). *$p < 0.05$, ** $p < 0.01$, **** $p < 0.0001$ (unpaired t test).

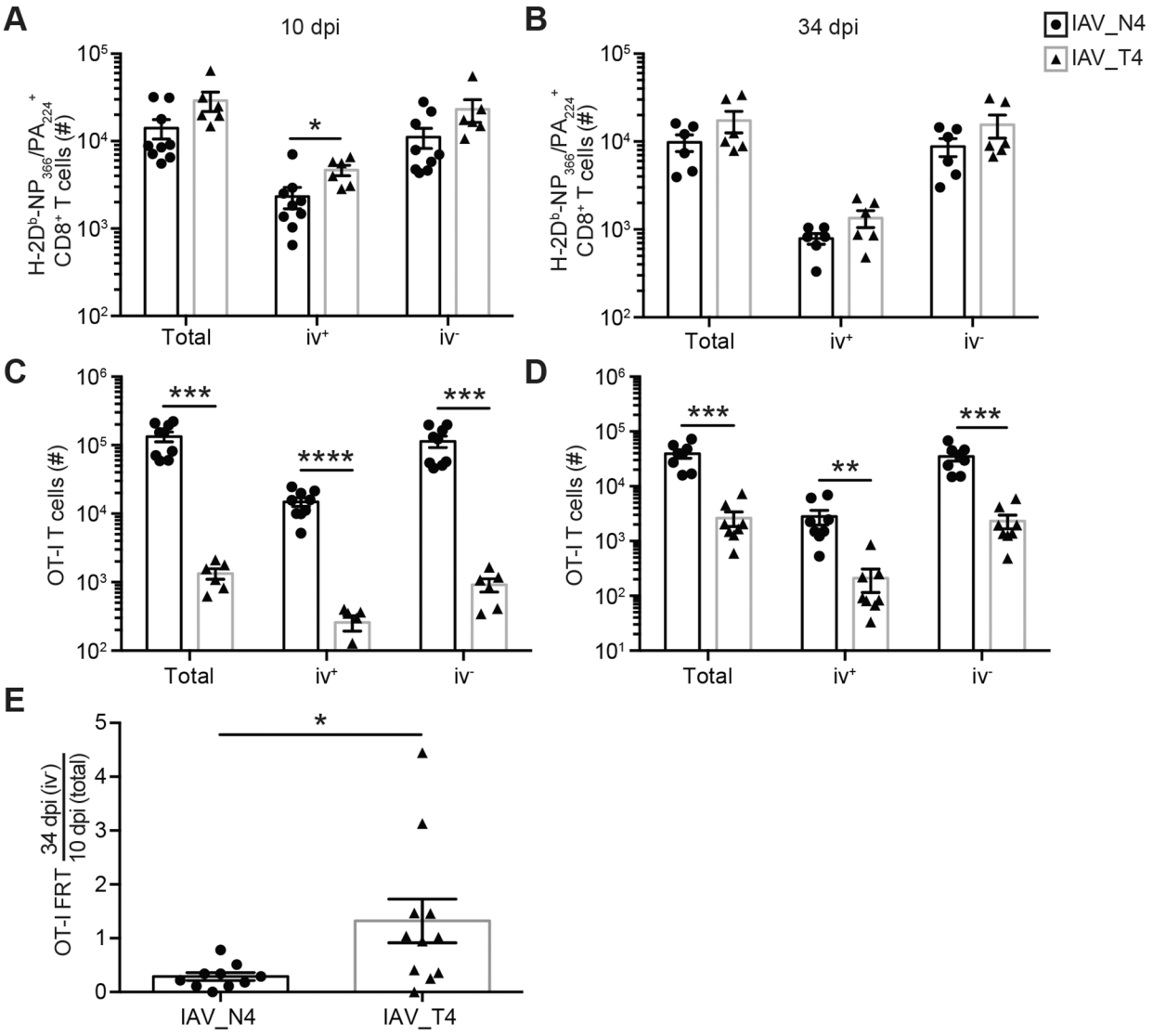

Figure 3. TCR signal strength alters T_{RM} formation in a distal uninfected mucosal tissue.

Challenged mice were generated as in Figure 1. On indicated dpi, FRTs were harvested after anti-CD8α iv injections. (**A, B**) The number of endogenous ($CD45.1^-$ $CD45.2^+$) $CD8^+$ H-$2D^b$-PA_{224}/NP_{366} tetramer$^+$ $CD44^{hi}$ cells, either total, iv^+, or iv^- cells in the FRT from mice infected with IAV_N4 or IAV_T4 at 10 (**A**) or 34 (**B**) dpi. (**C, D**) The number of OT-I T cells in the FRT at 10 (**C**) or 34 (**D**) dpi. (**E**) The number of iv^- OT-I T cells in the FRT at 34 dpi was divided by the average number of total OT-I T cells in the FRT at 10 dpi. The results (**A-E**) are representative of 2 independent experiments with at least 3 mice per group (± SEM). *$p < 0.05$, ** $p < 0.01$, *** $p < 0.001$, **** $p < 0.0001$ (unpaired t test).

Figure 4. TCR affinity simulation correlates with the differentiation status of OT-I T cells.

Challenged mice were generated as in Figure 1. (**A**) Representative flow plots of CD62L and CD44 staining of total splenic OT-I T cells from mice infected with IAV_N4 (left) or IAV_T4 (right) at 34 dpi. (**B**) The percentage of $CD44^+$ $CD62L^+$ (T_{CM}) or $CD44^+$ $CD62L^-$ (T_{EM}) OT-I T cells. (**C, E**) Representative flow plots of CD127 and KLRG1 staining of total splenic (top) or iv^- lung OT-I T cells (bottom) at 10 (**C**) and 34 (**E**) dpi with IAV_N4 or IAV_T4. (**D, F**) The percentage of total splenic (left) or iv^- lung (right) $KLRG1^+$ $CD127^-$ or $KLRG1^-$ $CD127^+$ OT-I T cells at 10 (**D**) and 34 (**F**) dpi. (**G**) Representative flow plots of CX_3CR1 staining of total splenic (top) or iv^- lung OT-I T cells at 34 dpi. Naïve host $CD44^{lo}$ cells are included for reference. Dashed line indicates gates. (**H, I**). The percentage of total splenic (**H**) or iv^- lung (**I**) OT-I T cells that $CX_3CR1^{neg,\ int\ or\ high}$ at 34 dpi. The results (**B**)

are compiled from 2 independent experiments with at least 4 mice per group, per experiment (± SEM). The results (**D, F**) are representative of 2 independent experiments, with at least 4 mice per group. The results (**H, I**) are from 1 experiment with 3–4 mice per group. *$p < 0.05$, ** $p < 0.01$, *** $p < 0.001$ (unpaired t test).

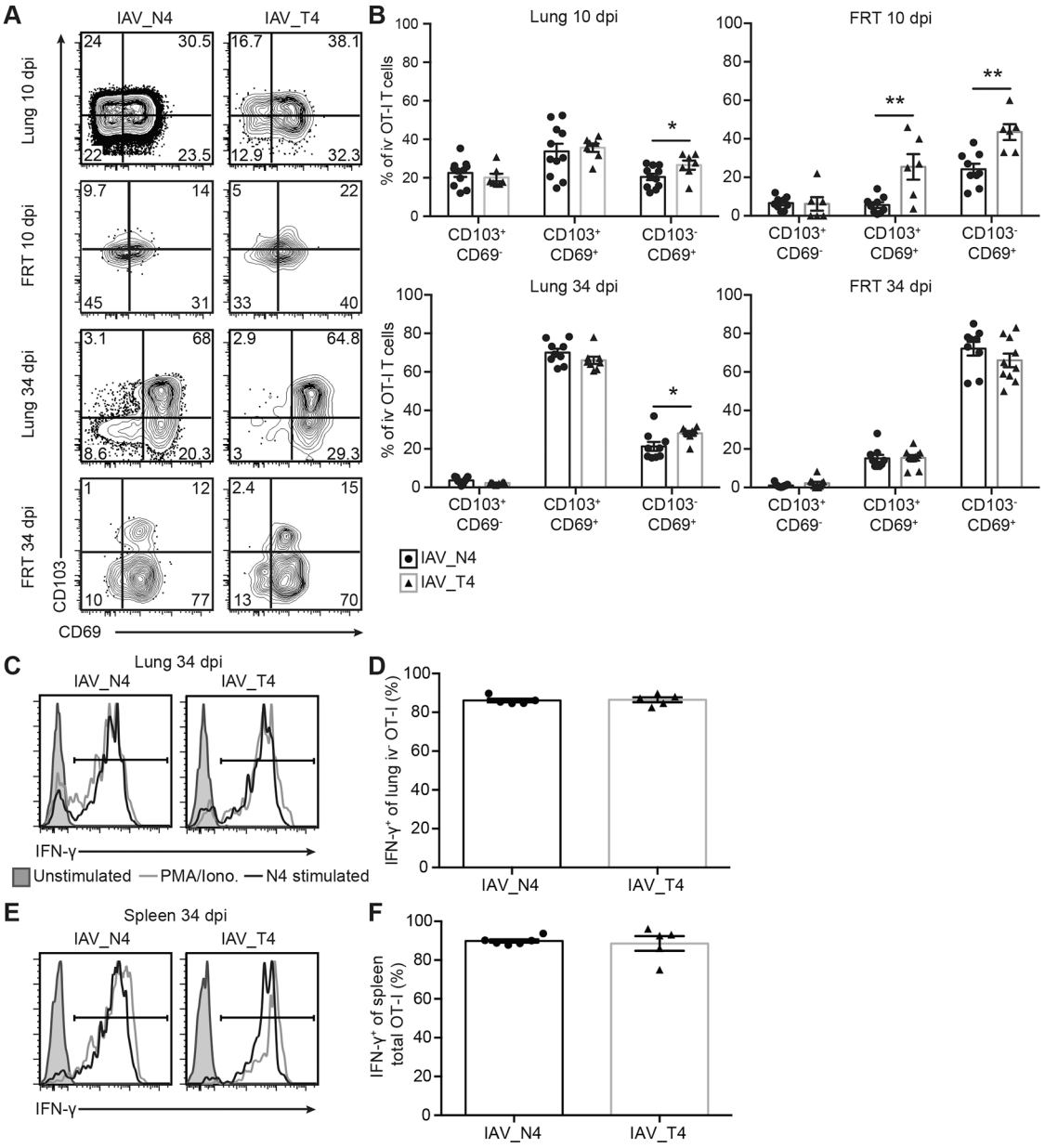

Figure 5. Phenotype of lung T_{RM} cells is independent of TCR signal strength.

Challenged mice were generated as in Figure 1. (**A**) Representative flow plots of CD69 and CD103 staining on iv$^-$ OT-I T cells in the lung and FRT on 10 and 34 dpi from mice. (**B**) The percentage of iv$^-$ OT-I T cells expressing CD103$^+$CD69$^-$, CD103$^+$CD69$^+$ or CD103$^-$CD69$^+$ (**C-F**) On 34 dpi, lungs (**C, D**) and spleens (**E, F**) were harvested and cells were stimulated *ex vivo* with 1 μg/mL N4 peptide. As a positive control, cells were stimulated with PMA/Ionomycin. (**C, E**) Representative IFN-γ staining of iv$^-$ lung (**C**) or total spleen (**E**) OT-I T cells unstimulated, stimulated with PMA/Ionomycin or N4 peptide. (**D, F**) Percentage of iv$^-$ lung (**D**) or total spleen (**F**) IFN-γ$^+$ OT-I T cells after *ex vivo* N4 stimulation. The results (B) are combined from 2 independent experiments with at least 3 mice per group, per experiment (± SEM). The results (D,F) are 1 representative experiment

of 2 independent experiments with at least 5 mice per group, per experiment (± SEM). *$p < 0.05$, ** $p < 0.01$ (unpaired t test).

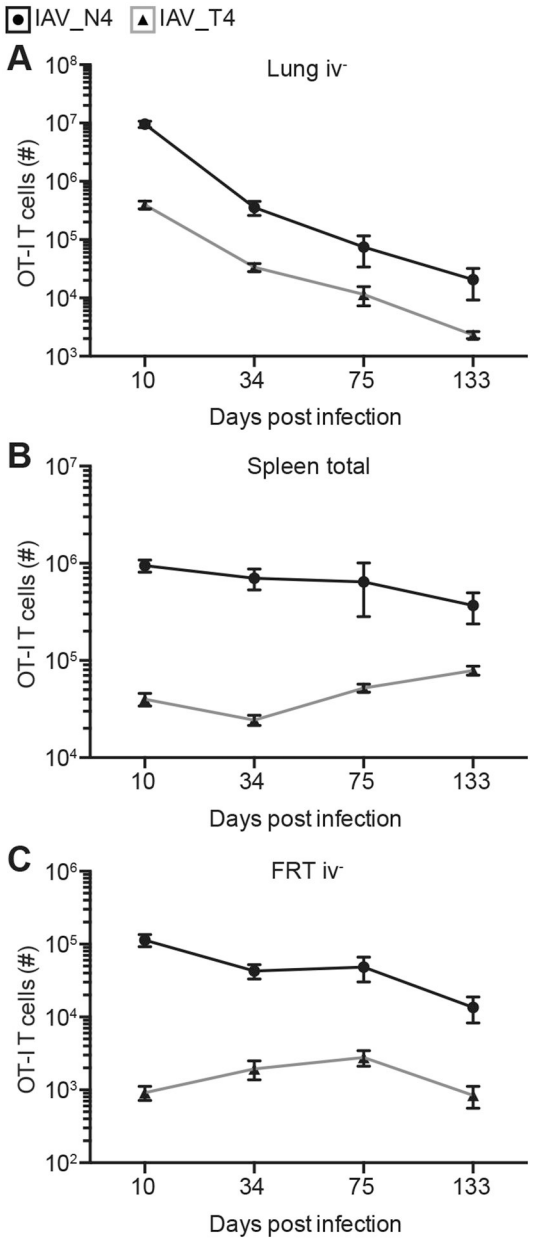

Figure 6. T_{RM} longevity is independent of TCR affinity.

Challenged mice were generated as in Figure 1. On indicated dpi, lungs (**A**), spleen (**B**) and FRTs (**C**) were harvested after anti-CD8α iv injections from mice infected with IAV_N4 or IAV_T4. The results (75 and 133 dpi) are of 1 experiment with at least 4 mice per group (± SEM). The data graphed for 10 and 34 dpi are shown in Figures 1 and 3.

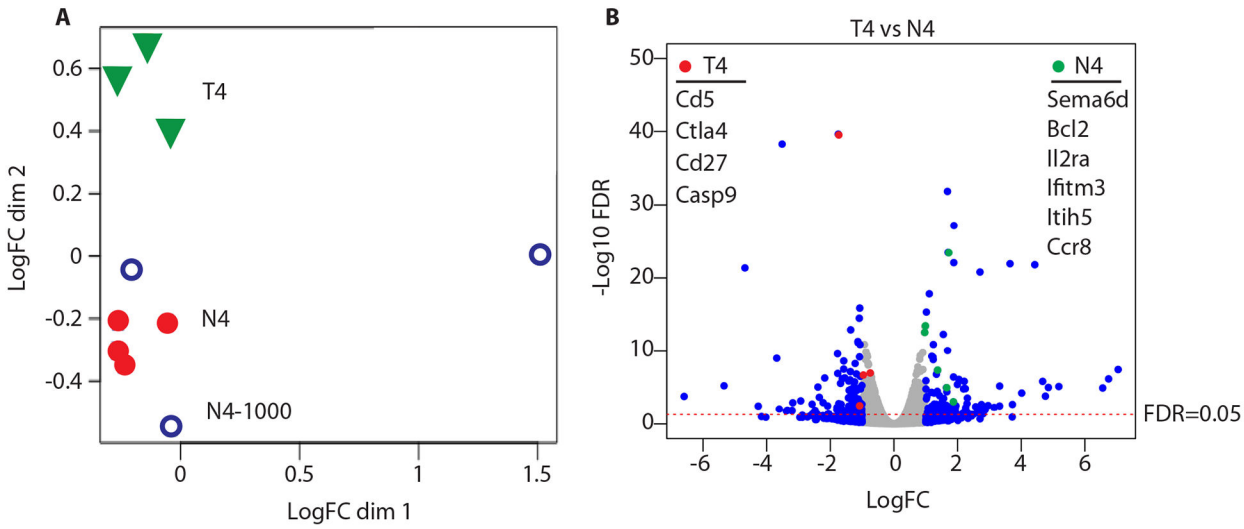

Figure 7. Transcriptional changes in low and high affinity T_{RM}.

Challenged mice were generated as in Figure 1. CD45.1^{+} OT-I CD8^{+} T cells were purified by FACS and RNA profiled by mRNA-seq. (**A**) Multidimensional scaling plot demonstrating transcript alterations between groups. (**B**) Volcano plot comparing expression changes between IAV_N4 and IAV_T4 primed OT-I T cells, dotted line FDR=0.05. Blue symbols ± 1 Log2FC. Genes highlighted by red and green circles are listed by Log10 FDR.